INL/CON-18-44290-Revision-0

Pronghorn: A Porous Media Thermal-Hydraulics Core Simulator and its Validation with the SANA Experiments

L. Zou, J.W. Peterson, R.C. Martineau, R.N. Slaybaugh, A. J. Novak

April 2018

The INL is a U.S. Department of Energy National Laboratory
operated by Battelle Energy Alliance

INL/CON-18-44290-Revision-0

Pronghorn: A Porous Media Thermal-Hydraulics Core Simulator and its Validation with the SANA Experiments

L. Zou, J.W. Peterson, R.C. Martineau, R.N. Slaybaugh, A. J. Novak

April 2018

Idaho National Laboratory
Idaho Falls, Idaho 83415

http://www.inl.gov

Prepared for the
U.S. Department of Energy

Under DOE Idaho Operations Office
Contract DE-AC07-05ID14517

Pronghorn: A Porous Media Thermal-Hydraulics Core Simulator and its Validation with the SANA Experiments

A.J. Novak[*], L. Zou[+], J.W. Peterson[+], R.C. Martineau[+], and R.N. Slaybaugh[*]

[*]*University of California, Berkeley, CA 94708*
[+]*Idaho National Laboratory, Idaho Falls, ID 83401*

Pebble bed High Temperature Reactors (HTRs) are characterized by many advantageous design features, such as excellent passive heat removal in accidents, large margins to fuel failure, and online refueling potential. However, a significant challenge in the core modeling of pebble bed reactors is the complex fuel-coolant structure. This paper presents a new porous media simulation code, Pronghorn, that aims to alleviate modeling challenges for pebble bed reactors by providing a fast-running, medium-fidelity core simulator. Pronghorn is intended to accelerate the design and analysis cycle for pebble bed and prismatic HTRs by permitting fast scoping studies and providing boundary conditions for systems-level analysis. Pronghorn is built on the Multiphysics Object-Oriented Simulation Environment (MOOSE) using modern software practices and a thorough testing framework. This paper describes the physical models used in Pronghorn and demonstrates Pronghorn's capability for modeling gas-cooled pebble bed HTRs by presenting simulation results obtained for the German SANA pebble bed decay heat experiments. Within the limitations of the porous media approximation and existing available closure relationships, Pronghorn predicts the SANA experimental pebble temperatures well, expanding the code's validation base. A brief code-to-code comparison shows a level of accuracy comparable to other porous media simulation tools. Pronghorn's advantages over these related tools include: an arbitrary equation of state, unstructured mesh capabilities, compressible flow models, the ability to couple to MOOSE fuels performance and systems-level thermal-hydraulics codes, and modern software design.

I. INTRODUCTION

Pebble bed High Temperature Reactors (HTRs) are expected to display excellent heat removal characteristics in operational and accident scenarios due to graphite's capability for storing and transferring heat, the very high failure temperatures of particle fuel, and the low power densities involved. However, a major challenge associated with the modeling of pebble bed reactors is the complex fuel-coolant structure in the core. Hundreds of thousands of fuel pebbles make full-core Computational Fluid Dynamics (CFD) simulations too expensive, while the lack of a natural subchannel makes subchannel codes difficult to adapt. By averaging the flow equations in space and providing additional closure relationships to express the effect of a porous solid matrix of fuel on the coolant, porous media models can provide medium-fidelity simulation results in reasonable run times to facilitate accelerated design and analysis. Both the lengthy mesh generation process required for CFD, and the correspondingly long run times, are alleviated through the use of a porous media model[1]. Porous media models cannot capture flow details around the pebbles and the highly asymmetric drag and heat transfer in the bed, but for the purposes of engineering-scale analysis, porous media models generally predict the fluid flow and fluid-solid heat transfer fairly well[1,2].

Pronghorn is a Finite Element (FE), porous media thermal-hydraulics simulation code built on the Multiphysics Object-Oriented Simulation Environment (MOOSE) framework[3] that is intended to provide simulation results in short turnaround times for design scoping studies, or core boundary conditions for systems-level analysis of pebble bed HTRs. An advantage associated with software built on the MOOSE framework is that all applications share a common code base, which facilitates relatively easy coupling. This leverages the many domain-specific man-hours dedicated to individual physics codes to be combined for sophisticated multiphysics analysis.

Pronghorn began development in 2008, but due to recent changes in the MOOSE framework and improved porous media models, was recently redeveloped from scratch. This paper presents an introduction to the models used in this modernized Pronghorn and its validation with the SANA pebble bed experiments[4] conducted in Germany from 1994-1996. The remainder of this report is organized as follows. Section II discusses the physical models used in Pronghorn; Section III introduces the SANA experiments and provides justification of several key modeling assumptions made; Section IV presents a brief overview of Pronghorn's verification framework and

modern software practices; Section V presents Pronghorn simulation results for several of the SANA experiments and a comparison with results obtained with comparable porous media codes; Section VI provides conclusions.

II. PHYSICAL MODELS

Numerical solutions to the fluid flow equations for Reynolds numbers of interest for nuclear reactor applications are very computationally expensive due to the need to resolve thin boundary layers, capture fine-scale turbulent motions, and, depending on the numerical method, ensure stability. This computational cost can be prohibitive to accelerated design and analysis of engineering-scale phenomena such as reactor response to a loss of offsite power. Provided the global impact of local variation in the fluid flow can be approximated, a simpler set of equations can be solved to predict reactor response. Porous media models, of common use in the chemical and geological engineering fields, approximate a solid-fluid medium as a two-phase mixture of solid and fluid, where the porosity ε reflects the fraction of a representative volume that is fluid,

$$\varepsilon = \frac{\text{fluid volume}}{\text{total volume}}. \quad (1)$$

The porosity in a cylindrical packed bed of spheres is a damped oscillatory function of the distance from the bounding wall[5]. At the wall, the porosity is nearly unity due to point contacts with the wall. Within four to five pebble diameters of the wall, the porosity reaches its bed average value that is typically in the range of 0.35-0.45 for beds of spheres. This large variation induces several important effects on the fluid flow. The pressure drop decreases approximately linearly with porosity, and a 1% change in porosity in the classic Ergun drag correlation produces about a 10% change in the local pressure drop[6]. The lower-porosity region near the bounding walls therefore leads to a flow-channeling effect. Velocities near the wall are about 2-3 times higher than in the center of the bed[7]. The variation of pressure drop with porosity is approximated by a porous medium friction factor, W.

In addition to porous media drag, the porosity influences the convective and conductive heat transfer in the bed. Lower porosities yield improved convective heat transfer due to the more tortuous fluid paths. The convective heat transfer coefficient α decreases approximately linearly with porosity. While the correlation between porosity and convective heat transfer coefficient is not as strong as the correlation between porosity and pressure drop, a 1% change in the porosity produces about a 3% change in the local convective heat transfer coefficient[6]. Finally, the solid conductive heat transfer, represented by an effective solid thermal conductivity κ_s, is also a function of porosity. While conduction occurs within each solid pebble, heat transfer also occurs through pebble contact areas and by radiation and conduction across fluid gaps. Higher porosities therefore lead to improved radiation heat transfer, but reduced contact conduction[8].

The porous media versions of the fluid flow equations are derived by averaging the equations over a representative volume consisting of a mixture of solid and fluid[9]. This averaging process produces several constitutive terms that are not normally present in the governing equations. The governing equations used for simulation of the SANA facility are discussed in Section II.A, followed by the semi-empirical and empirical correlations developed for porous media closure terms in Section II.B, and finally the thermophysical fluid and solid properties in Section II.C.

II.A. Governing Equations

Pronghorn solves the porous media equivalents of the Euler equations for the fluid pressure P, momentum $\rho_f \vec{V}$, and temperature T_f, and the porous media solid energy equation for solid temperature T_s. A detailed derivation and description of these governing models and closure relationships is beyond the scope of this paper, but can be found elsewhere[10]. Several additional assumptions are made beyond those associated with the Euler equations that are acceptable for slowly-evolving transients. Ongoing work involves numerical stabilization that will permit full-core solutions with the porous media Euler equations. All of the equations presented in this section are obtained by averaging the governing equations over a representative elementary volume consisting of solid and fluid. The conservation of momentum equation is

$$\frac{\partial(\varepsilon\rho_f\vec{V})}{\partial t} + \nabla\cdot\left(\varepsilon\rho_f\vec{V}\vec{V}\right) + \varepsilon\nabla P - \varepsilon\rho_f\vec{g} + W\rho_f\vec{V} = 0, \quad (2)$$

where ρ_f is the fluid intrinsic density, $\vec{V}$ is the fluid intrinsic velocity, and $\vec{g}$ is the gravitational acceleration vector. By neglecting the time rate of change of momentum and the advection of momentum, the momentum conservation equation simplifies to

$$\varepsilon\nabla P - \varepsilon\rho_f\vec{g} + W\rho_f\vec{V} = 0\,. \quad (3)$$

This form of the momentum equation is valid for low Reynolds number flows and slowly-evolving transients, since changes in momentum are instantaneously reflected as changes in pressure. Because drag effects are about 1000 times more significant than advection effects in low-flow gas-cooled pebble bed reactors[11], neglecting the advection of momentum is justified for the SANA experiments. However, as mentioned, ongoing work focuses on improving stabilization such that momentum

advection need not be neglected. Eq. (3) is solved for fluid momentum. The conservation of mass equation is

$$\frac{\partial(\varepsilon\rho_f)}{\partial t} + \nabla \cdot \left(\varepsilon\rho_f \vec{V}\right) = 0\,. \tag{4}$$

Eq. (4) can be transformed to a diffusive equation by rearranging Eq. (3) for momentum and substituting into Eq. (4), giving a pressure Poisson equation,

$$\frac{\partial(\varepsilon\rho_f)}{\partial t} + \nabla \cdot \left[\frac{\varepsilon^2}{W}\left(-\nabla P + \rho_f \vec{g}\right)\right] = 0\,. \tag{5}$$

Eq. (5) is solved for the fluid pressure, and the fluid density is provided by an Equation of State (EOS) corresponding to e.g. ideal gas, stiffened gas, barotropic fluid, etc. This flexibility alleviates the ideal gas EOS restrictions of many earlier porous media codes.

The fluid temperature equation is derived from the conservation of total energy equation using equilibrium thermodynamics. Neglecting compression work and viscous heating gives

$$\rho_f c_{pf} \frac{\partial(\varepsilon T_f)}{\partial t} + \varepsilon\rho_f c_{pf} \vec{V} \cdot \nabla T_f - \nabla \cdot \left(\kappa_f \nabla T_f\right) + \alpha\left(T_f - T_s\right) + \dot{q}_f = 0, \tag{6}$$

where c_{pf} is the fluid isobaric specific heat, T_f is the intrinsic fluid temperature, κ_f is the effective fluid thermal conductivity, T_s is the intrinsic solid temperature, and $\dot{q}_f$ is a heat source in the fluid. Eq. (6) is solved for the fluid temperature. The same derivation is performed for the solid energy equation, giving

$$\rho_s c_{ps} \frac{\partial((1-\varepsilon)T_s)}{\partial t} - \nabla \cdot (\kappa_s \nabla T_s) + \alpha\left(T_s - T_f\right) + \dot{q}_s = 0, \tag{7}$$

where ρ_s is the solid intrinsic density, c_{ps} is the solid isobaric specific heat, κ_s is the effective solid thermal conductivity, and $\dot{q}_s$ is the heat source in the solid. Eq. (7) is solved for the solid temperature. Because the heat source in the SANA experiments is not a volumetric source and the pebbles contain no fissile material, $\dot{q}_f$ and $\dot{q}_s$ are zero. The solid phase is assumed to be stationary and incompressible, therefore no conservation of mass or momentum equations are required for this phase.

II.A.1 Numerical Method

The governing equations are solved using the Finite Element Method (FEM). By multiplying each equation by a test function and applying integration by parts when possible, the weak form of each equation is derived. The derivation of these weak forms is given in detail elsewhere[10].

After spatial discretization by the FEM, the Jacobian Free Newton Krylov (JFNK) method is used to solve the system of coupled, nonlinear equations[12]. This solution method requires an outer loop over Newton iterations, and an inner loop over linear iterations. The Jacobian required for the Newton iterations is approximated with a first-order accurate finite difference derivative. The linear iterations are performed using the Generalized Minimal Residual Method (GMRES) method[13]. The Method of Lines temporal discretization method is used. Both explicit and implicit time discretization schemes are available in MOOSE; only implicit schemes are used in the present work.

II.A.2 Boundary Conditions

Two general types of Boundary Conditions (BCs), Dirichlet and Neumann, can be specified in Pronghorn. A Dirichlet BC strongly enforces a known value for a variable on a boundary. Neumann BCs arise from the FE integration by parts discussed in Section II.A.1, and allow the user to weakly enforce a specified flux (such as heat flux) at the boundary.

For hyperbolic equations, because information travels along characteristics, some BCs can only be specified on inflow boundaries. Special "free" BCs are needed on outflow boundaries to avoid the default zero-Neumann BC arising from the FE discretization. In the discussion of BCs that follows, the i and o subscripts indicate known inlet and outlet values, and in, out, and $wall$ indicate inflow, outflow, and solid wall boundaries. $\partial\Omega$ indicates a boundary, and $\vec{n}$ is the unit outward normal for that boundary. The Neumann-type BC for the pressure Poisson equation is

$$\frac{\varepsilon^2}{W}\left(-\nabla P + \rho_f \vec{g}\right) \cdot \vec{n} = \begin{cases} \rho_{fi}\vec{V}_i \cdot \vec{n} & \partial\Omega_{in} \\ \rho_f \vec{V} \cdot \vec{n} & \partial\Omega_{out} \\ 0 & \partial\Omega_{wall} \end{cases}. \tag{8}$$

Because the pressure Poisson equation is parabolic in nature, a Dirichlet BC for pressure can be specified on any boundary, provided a Neumann BC is not also specified on that boundary. This Dirichlet BC is commonly specified on the outflow so that an inlet momentum can still be specified. Hence, a Dirichlet pressure BC can be specified on $\partial\Omega_{out}$ instead of the $\partial\Omega_{out}$ condition shown in Eq. (8).

No BCs are required for the momentum equation. For the fluid energy equation, a Dirichlet value for fluid temperature can be specified on any boundary. The Neumann BCs for the fluid energy equation are

$$-\kappa_f \nabla T_f \cdot \vec{n} = \begin{cases} \tilde{q}_f & \partial\Omega_{\text{heat flux}} \\ h_{wall}\left(T_f - T_{wall}\right) & \partial\Omega_{\text{convection}} \end{cases}, \tag{9}$$

where $\tilde{q}_f$ is a known value of heat flux, h_{wall} is the convective heat transfer coefficient between the fluid and

a bounding wall, and T_{wall} is the known wall temperature. Radiation heat transfer between the fluid and the surroundings is neglected, as the solid temperature for reactor applications will be significantly larger than the fluid temperature.

For the solid energy equation, a Dirichlet value for solid temperature can be specified on any boundary. The Neumann-type BCs for the solid energy equation are

$$-\kappa_s \nabla T_s \cdot \vec{n} = \begin{cases} \tilde{q}_s & \partial\Omega_{\text{heat flux}} \\ \epsilon_w \sigma (T_s^4 - T_\infty^4) + h_{NC}(T_s - T_\infty) & \partial\Omega_{\text{rad + conv}} \end{cases}, \quad (10)$$

where $\tilde{q}_s$ is a known value of heat flux, ϵ_w is the emissivity of the wall, σ is the Stefan-Boltzmann constant, h_{NC} is the natural convection coefficient between the outer wall and the ambient, and T_∞ is the ambient temperature. The BCs for the SANA experiments are described in Section III.B.

II.B Porous Media Closure Relationships

ε, W, α, κ_f, and κ_s are additional terms that appear in the averaging process that are required to express the drag and heat transfer characteristics of the porous medium. Because the governing equations discussed in the previous section become stiff near the walls where porosity approaches unity[7], and because wall channeling effects generally only have local impacts on the overall bed solution[14], a constant porosity of 0.4 is assumed for the SANA benchmarks as a first approximation, though Pronghorn does include capabilities for spatially-dependent porosity.

The friction factor W represents the sum of the Darcy and Forchheimer drag coefficients. The Darcy drag is linearly proportional to velocity, and hence represents friction drag in laminar flows. At higher Reynolds numbers, though still in the laminar regime, inertial effects such as expansion/contraction through pores and fluid bending induces a quadratic velocity dependence that is captured by the Forchheimer model. In the turbulent regime, a drag reduction effect is often observed relative to the laminar drag[15,16]; for gas-cooled pebble beds, KTA provides a correlation for the overall drag that uses a Reynolds-number-dependent Forchheimer drag[17],

$$W = \frac{160(1-\varepsilon)^2}{\varepsilon d^2}\frac{\mu_f}{\rho_f} + 3\left(\frac{1-\varepsilon}{Re}\right)^{0.1}\frac{(1-\varepsilon)|\vec{V}|}{d}, \quad (11)$$

where μ_f is the fluid viscosity and Re is the Reynolds number based on the extrinsic velocity and pebble diameter d. Eq. (11) is valid for $1 < Re/(1-\varepsilon) < 10^5$ and $0.36 < \varepsilon < 0.42$. KTA also provides the convective heat transfer coefficient for beds of spherical pebbles[18],

$$Nu = 1.27\frac{Pr^{1/3}Re^{0.36}}{\varepsilon^{1.18}} + 0.033\frac{Pr^{0.5}Re^{0.86}}{\varepsilon^{1.07}}, \quad (12)$$

where Nu is the Nusselt number based on d and Pr is the Prandtl number. Eq. (12) is valid for $100 < Re < 10^5$ and $0.36 < \varepsilon < 0.42$. The volumetric heat transfer coefficient is obtained by multiplying the solid surface area per unit volume, which for a bed of spheres gives[5]

$$\alpha = \frac{6(1-\varepsilon)}{d}\frac{k_f Nu}{d}, \quad (13)$$

where Nu is given by Eq. (12). For heat transfer between the bed and the walls[5],

$$Nu_{wall} = \left(1 - \frac{d}{D}\right) Re^{0.61} Pr^{1/3}, \quad (14)$$

where D is the bed diameter. After heat is transferred to the wall, it is conducted through the wall and is finally transferred to the ambient by natural convection, which can be approximated by correlations developed for natural convection from a vertical flat plate.

κ_f represents the effective fluid thermal conductivity. For simplicity, this is simply taken as

$$\kappa_f = \varepsilon k_f, \quad (15)$$

which assumes that the only reduction in conductive heat transfer occurs due to flow area reduction. More accurate models for κ_f that account for the tortuosity of the medium and the enhancement of thermal energy dispersion due to fluctuations in velocity and temperature due to interactions with the porous solid are ongoing[19].

κ_s represents the combined effects of solid-to-solid radiation, solid-fluid-solid conduction, and solid-solid conduction via pebble contact areas. A modified Zehner-Bauer-Schlunder correlation[20] is used for κ_s, with Knudsen effects in the fluid neglected and the fluid assumed transparent to thermal radiation,

$$\kappa_s = k_f\left(1 - \sqrt{1-\varepsilon}\right)(1 + \varepsilon\varkappa_R) + k_f\sqrt{1-\varepsilon}(\varphi\lambda + (1-\varphi)\varkappa_{SF}), \quad (16)$$

where φ is the contact area fraction[8], λ is the solid-to-fluid thermal conductivity ratio, $\varkappa_R$ is the effective thermal conductivity due to radiation, and $\varkappa_{SF}$ is given by

$$\varkappa_{SF} = \frac{2}{a}\left[\frac{\lambda+\varkappa_R-1}{a^2\lambda/B}\ln\frac{\lambda+\varkappa_R}{B} - \frac{B-1}{a} + \frac{B+1}{2B}(\varkappa_R - B)\right]. \quad (17)$$

The remaining numerical factors a and B are given as

$$a = \left(1 + \frac{\varkappa_R - B}{\lambda}\right), \quad (18)$$

and

$$B = 1.25\left(\frac{1-\varepsilon}{\varepsilon}\right)^{10/9}. \quad (19)$$

The radiation component indicated by $\varkappa_R$ is set to zero in order to permit the use of a different correlation, and is instead computed by

$$\kappa_{rad} = \frac{k_s}{\Lambda}\left[\left(1-\sqrt{1-\varepsilon}\right)\varepsilon\right] + \frac{k_s}{\Lambda}\left[\frac{\sqrt{1-\varepsilon}}{2/\epsilon_s-1}\frac{B+1}{B}\frac{1}{1+1/\left((2/\epsilon_s-1)\Lambda\right)}\right] \quad (20)$$

for easier comparison with the models used in THERMIX[21,22], where ϵ_s is the emissivity of the pebbles and Λ is

$$\Lambda = \frac{k_s}{4\sigma T_s^3 d}. \quad (21)$$

Then, κ_s is computed as the sum of Eqs. (20) and (16), where $\varkappa_R$ is set to zero in Eq. (16). The closure relationships presented in this section are all specific to pebble bed reactors. Pronghorn includes more options for the required pebble bed closure models – a discussion can be found in the theory manual[10]. Future work is intended to expand Pronghorn's application space to include prismatic-type reactors.

II.C Thermophysical Properties

Correlations for helium density, viscosity, thermal conductivity, and a constant value for specific heat are obtained from the literature[23]. These correlations are valid over a wide range of pressures and temperatures.. A generalized fluid properties module is under development in MOOSE, and to avoid duplicating those efforts, constant values of $\mu_f = 3.5932\times10^{-5}$ Pa · s, $k_f = 0.055197$ W/m·K, and $c_{pf} = 1122.3$ J/kg·K are used for nitrogen, while the ideal gas law is used for density.

For graphite properties, tabulated data for thermal conductivity and density are provided with the SANA documentation[4]. Graphite specific heat is obtained from the literature[24]. The graphite emissivity, Young's modulus, and Poisson ratio are taken as 0.8, 9×10^9 Pa, and 0.136, respectively[22].

III. THE SANA FACILITY

The SANA facility consists of a cylindrical steel vessel containing about 9500 spherical graphite pebbles. The bed is heated by one to four electrical resistance heater elements, and the temperature is measured throughout the bed with thermocouples. Either nitrogen, helium, or argon gas flows through the bed at low velocities on the order of 10^{-5} m/s. About 40 cm of insulation is present at the top and bottom of the bed. The maximum power density of 28 kW/m^3 corresponds to 0.93% of the full power of a typical HTR design. Over 50 experiments were completed, though the present work focuses only on the simulation of six of these experiments. All of these experiments use a single, long, central heater and graphite pebbles with steady state conditions. Table 1 shows case letters that will be used to refer to these six experiments throughout this report.

TABLE I. Summary of SANA experiments completed in the present work and case letters for easy reference.

Case	Coolant	Nominal Power (kW)
A	helium	10.00
B	helium	20.00
C	helium	35.10
D	nitrogen	10.03
E	nitrogen	20.00
F	nitrogen	24.97

III.A Geometrical Modeling Assumptions

Because no significant azimuthal asymmetries exist with the selected cases, Pronghorn is run in a 2-D cylindrically symmetric geometry. It should be noted that, due to the flexibility of the FEM, Pronghorn can in general run on 3-D, unstructured meshes. For simplicity, only the core itself is modeled. The presence of the upper and lower insulation layers, the central heater, and the vessel wall is approximated through the BCs discussed in Section III.B.

III.B Boundary Condition Selection

The central heater is not modeled explicitly, but is treated as a known heat flux boundary, with heat flux given by the power divided by the heater surface area, and is assumed to be uniform over the heater surface. This heat flux is assumed to be split amongst the solid and fluid in a $1-\varepsilon : \varepsilon$ ratio. Due to the large amount of insulation at the top and bottom of the bed, these boundaries are assumed insulated for the fluid and solid energy equations. At the outer wall, it is assumed that the fluid transfers its heat first to the solid phase, so that the fluid has an insulated boundary on the vessel wall. For this reason, h_{wall} is set to zero in the present work. The solid is assumed to transfer its heat directly to the ambient via natural convection and radiation, as no vessel wall is explicitly modeled. A constant $h_{NC} = 18.4$ W/m$^2\cdot$K is recommended[25] and is used in the present work. ϵ_w is assumed to be 1. Work is ongoing to develop more sophisticated solid boundary models using Eq. (14) and combined porous-nonporous media modeling.

The inlet and outlet velocity is set to zero due to the very low flow rates involved. A no-penetration velocity is set at the vertical walls. The initial pressure is taken to be 1 atm.

IV. VERIFICATION RESULTS

Before attempting any validation efforts, all of the physics models in Pronghorn were subjected to a rigorous verification and testing framework[10]. All spatially-dependent kernels, BCs, and constitutive relationships are required to show theoretical linear and quadratic element convergence rates using the Method of Manufactured Solutions (MMS) combined with mesh refinement studies in 2-D and 3-D. Over 300 individual tests have been created to ensure model correctness. The convergence rates calculated using the L^2-norm of the FE solution error is shown in Fig. 2 for the time-independent portion of Eq. (5). The expected convergence rates of 2 and 3 for linear and quadratic elements, respectively, are obtained. For time-dependent physics, four different time discretization schemes are selected, and a linear-in-space MMS solution is chosen such that the error introduced by the spatial discretization is essentially zero. Fig. 2 shows the temporal convergence study for the time derivative in Eq. (6). Expected rates of convergence are observed for all four time discretization schemes.

In addition to these rigorous testing requirements, Pronghorn is version controlled and modern software practices are employed in its development. All changes made to the master branch of the code require all the previously discussed MMS tests to provide the same simulation results as reference cases, thus maintaining code correctness in tandem with feature development[26]. Code formatting standards improve readability. Peer review of all merge requests ensures high code standards.

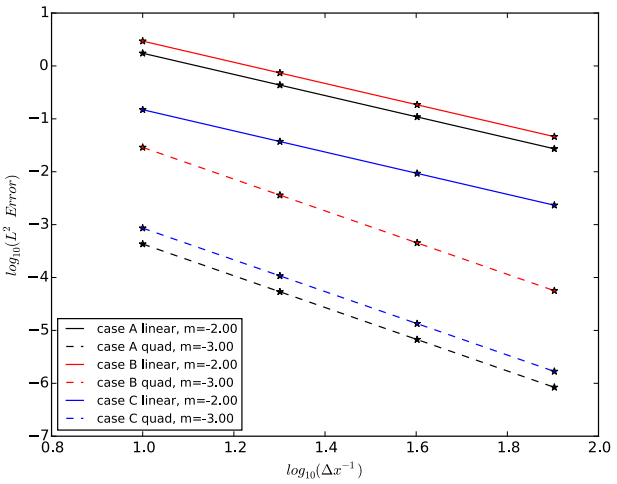

Fig. 1. Mesh convergence study for the time-independent portion of Eq. (5) for three different analytical solutions in 2-D. Convergence rates are shown as "m" in the legend.

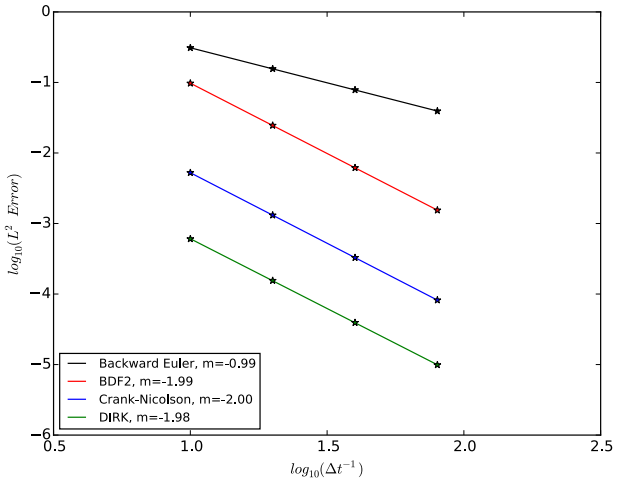

Fig. 2. Time step convergence study for the time-dependent kernel in Eq. (6) for four different time discretization methods. Convergence rates are shown as "m" in the legend.

V. SANA VALIDATION RESULTS

Prior to assessing results, mesh independence studies were conducted to ensure sufficiently refined meshes. After determining appropriate mesh refinements, to improve stability, each simulation is run as a transient until steady state is reached. Figs. 3-5 show Pronghorn radial solid temperature results for cases A, B, and C, respectively, at three different vertical elevations, z.

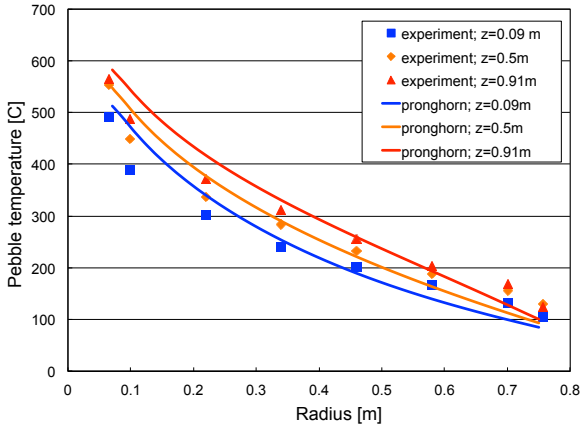

Fig. 3. Experimental and Pronghorn radial solid temperature at three different elevations for case A.

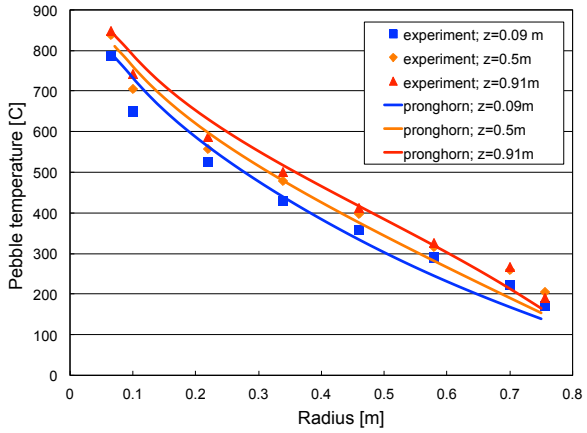

Fig. 4. Experimental and Pronghorn radial solid temperature at three different elevations for case B.

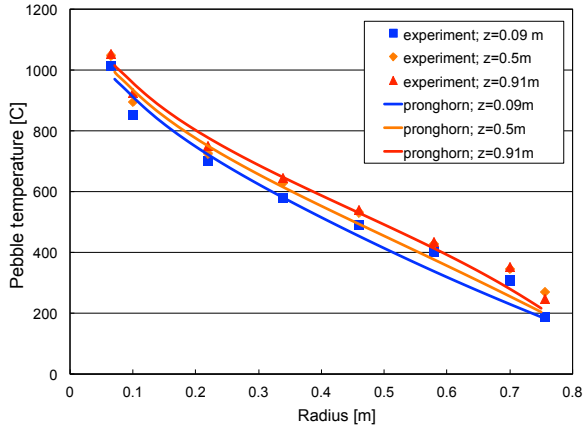

Fig. 4. Experimental and Pronghorn radial solid temperature at three different elevations for case C.

For these three helium cases, temperatures tend to be overpredicted near the center of the bed, and underpredicted near the outer periphery. Reasonable temperature predictions are obtained in the bulk of the bed. The largest errors occur for the lowest power case.

Figs. 6-8 show Pronghorn radial solid temperature results for cases D, E, and F, respectively, at the same three axial elevations. At 600°C and 1 atm, the thermal conductivity of helium is about 5.5 times larger than that of nitrogen. Because nitrogen does not conduct heat as efficiently as helium, a larger portion of the heat transfer occurs by natural convection. This causes the larger axial temperature gradients seen in Figs. 6-8 relative to Figs. 3-5.

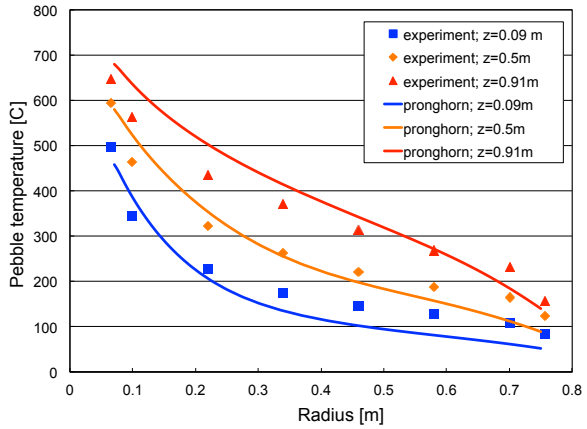

Fig. 6. Experimental and Pronghorn radial solid temperature at three different elevations for case D.

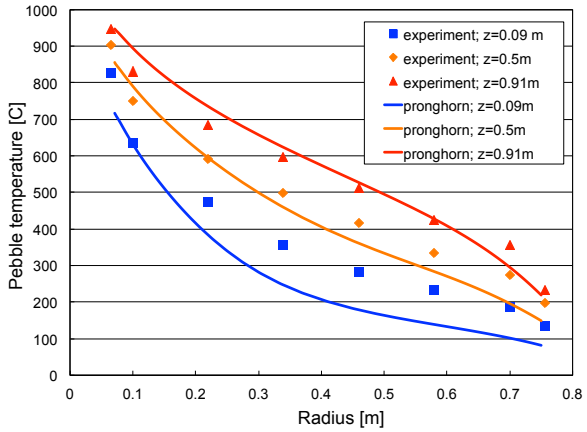

Fig. 7. Experimental and Pronghorn radial solid temperature at three different elevations for case E.

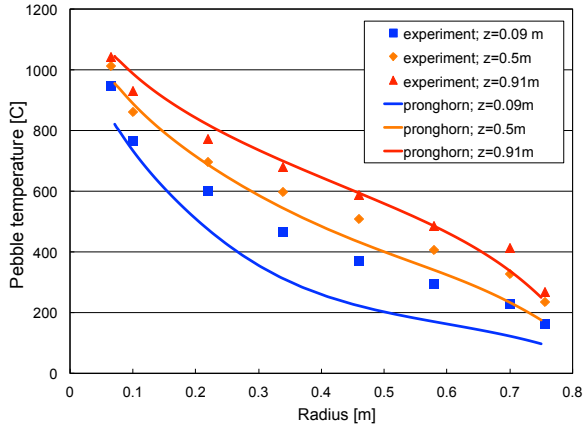

Fig. 8. Experimental and Pronghorn radial solid temperature at three different elevations for case F.

In general, the Pronghorn simulation results for nitrogen are less accurate than those for helium. Temperatures are generally underpredicted at the two

lowest elevations, but slightly overpredicted at the higher elevations. Contrary to the helium cases, the largest errors are generally in the bulk of the bed where the porous media assumption is the "most valid."

Fig. 9 shows velocity vectors for case A. Natural circulation flow is clearly visible, as the hot inner wall heats the fluid, causing it to rise in the inner bed region. The fluid is cooled in the outer bed region by natural convection and radiation heat transfer to the ambient, causing the fluid to flow downwards at the outer wall. A stagnation region forms about 2/3 of the radial distance from the center of the bed. No experimental velocity measurements are provided for comparison, but physically-realistic behavior is observed.

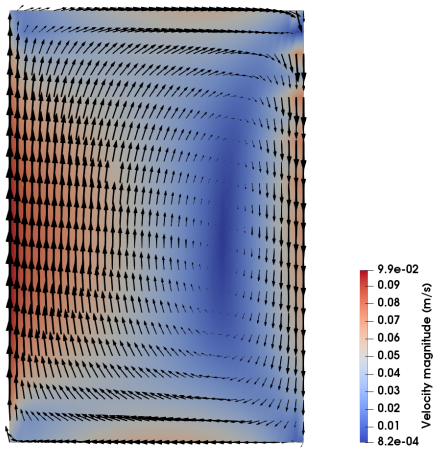

Fig. 9. Pronghorn velocity vector field, colored with velocity magnitude, for case A.

V.A Assessment of Modeling Errors

Many model improvements can be identified that would likely improve the simulation results presented here. The simulation results were found to be very sensitive to the correlation chosen for κ_s. For case A, a slightly different model[20] for the radiation component of κ_s gave temperatures 75°C higher in the center of the bed where the radiation transfer is most significant due to the high temperatures, than those shown in Fig. 3. Many other correlations for the radiation component of κ_s have been used for the SANA benchmarks in the literature. Several of these correlations better account for radiation heat transfer between distant regions of the bed[27]; future work will investigate these other models and their impact on accuracy in the highest-temperature regions of the bed.

The approximation that the core transfers its heat by natural convection directly to the ambient, rather than through the vessel wall, is likely the origin of the errors at the outer edges of the bed. Work is currently ongoing to add the capability to apply BCs between a porous media and a non-porous media such as a vessel wall to more accurately capture this conjugate heat transfer. Also, the assumption of a constant h_{NC} should be relaxed by implementing flat plate convection correlations. Errors at both the inner and outer edges of the bed can also be partially attributed to using a constant porosity[28]. Larger errors near the edges of a packed bed are also to be expected, simply due to the nature of the porous media assumption, which treats the packed bed as a continuum. Work is currently ongoing to develop stabilization schemes to aid in solving the stiff equations that result near the walls where porosity tends to unity.

The largest errors for helium are observed for the lowest-power cases. At low powers, natural convection heat transfer constitutes a greater fraction of the total heat transfer. The correlation used for α is only valid for $Re > 100$. Due to the very low flowrates involved, future work will focus on the implementation of natural convection heat transfer coefficient correlations. The largest errors for nitrogen are observed in the bulk of the bed and at the highest powers. In the bulk of the bed, the porous media approximation is the "most valid." This observation, and the fact that the high powers show larger variation in temperatures, and thus thermophysical properties, suggests that the errors in the nitrogen simulations are primarily due to the use of constant viscosity and thermal conductivity, rather than BCs or the use of constant porosity (both of which have a larger effect on the solution near the walls). Improved results will likely be obtained when the generalized fluid properties module in MOOSE becomes available.

For both helium and nitrogen, the largest errors are typically observed at the lowest elevation. This may be caused by the approximation of zero inlet velocity, but may also be due to the choice of heat transfer coefficient. There appears to be disagreement in the literature as to whether the convective heat transfer coefficient should be larger or smaller than the average bulk value in the entrance layers to the bed. Achenbach, as well as the KTA correlation for α, suggest that α is about two times smaller in the first few pebble layers in the bed[5,18]. On the other hand, CFD simulations have shown that α is about two times larger in the first few pebble layers than in the bulk of the bed[29]. Future investigations are needed to clarify this effect.

Finally, simulation results will be improved in general once thermal dispersion is implemented. A consistent stabilization scheme is nearing completion, which will allow the inclusion of the advection term in the momentum equation, which likely would not be significant for the very low flow rates in the SANA facility, but may be important for reactor analysis.

V.B A Brief Discussion of Other Benchmark Participant Results

A detailed code-to-code comparison of the SANA experiments is beyond the scope of this paper, but a brief discussion of comparable porous media simulation results is illustrative. ANSYS CFX[25], a legacy version of Pronghorn[30] (circa 2008), MGT-3D[25], THERMIX[22], TINTE[22], and TRIO-EF[22] are a selection of porous media codes that have computed one or more SANA experiment cases. Of these codes, the majority modeled the insulation layers and vessel wall. Several even included models of thermocouple casings and other small geometric features. Except for the present and legacy Pronghorn simulations, all codes used a spatially-varying porosity, usually a piecewise constant function that is constant in the bed, with a higher, still constant value, within a half pebble diameter of the bounding walls.

The present Pronghorn results improve upon the legacy Pronghorn results via the selection of BCs. The legacy simulation results specified Dirichlet values for fluid and solid temperatures using values measured in the experiments. This *a priori* knowledge of the solution is unrealistic to use when trying to assess a code's predictive capability. All of the BCs used in the present results do not assume any *a priori* knowledge of the solution, and hence are more representative of the way the code will be used in practice. In a similar vein, the MGT-3D and CFX results were obtained by fine-tuning the wall heat transfer coefficient and the emissivity within the gap of the resistance heater until good agreement with the experimental measurements was obtained[25], and then these two values were fixed for the remainder of the simulations. Because model calibration with experimental data is in general not possible, the BCs used in the present results yield a more accurate representation of predictive results that could be obtained by a realistic user.

Despite these differences in fidelity and assumptions, temperature variations on the order of 50-100°C in some locations are typical for all of the test codes. The CFX simulation, which includes a turbulence model, shows excellent results. This observation suggests the addition of turbulence models in Pronghorn may be a fruitful endeavor, as turbulence is currently only approximated through the correlations used for W and α. Based on the good agreement with other codes and the results presented in Section V, Pronghorn can model gas-cooled pebble beds reasonably well. Furthermore, we are confident that more accurate results will also be obtained once the future work outlined in Section V.A is undertaken.

VI. CONCLUSIONS

Porous media models of pebble bed reactors have runtimes about 1% or less than those of detailed CFD models and employ much simpler meshes[1]. At the expense of approximating the local flow and heat transfer effects, medium-fidelity simulations can be performed to accelerate the design process of advanced pebble bed HTRs. This paper has presented a new porous media thermal-hydraulics simulation code, Pronghorn. In addition to the advantages associated with porous media models in general, Pronghorn 1) permits an arbitrary EOS to allow future simulation of liquid-cooled HTRs, 2) can use unstructured meshes, 3) is based on modern software practices, and 4) is built on the MOOSE framework, which makes possible interesting multiphysics simulation studies incorporating nuclear fuels, systems-level thermal-hydraulics, and many other applications.

Essential to the development of any new simulation tool is the establishment of a strong validation base. This paper has introduced the models in Pronghorn and shown their validation with the SANA experiments. Future work involving numerical stabilization, higher-fidelity models, and generalized improvements to the MOOSE framework has been outlined with the goals of permitting widespread use of a fast and accurate thermal-hydraulics simulator for pebble bed and prismatic reactors.

ACKNOWLEDGMENTS

This material is based upon work supported under a Department of Energy Nuclear Energy University Programs Graduate Fellowship.

REFERENCES

1. C. Y. WU, Y. M. FERNG, C. C. CHIENG, and C. C. LIU, "Investigating the Advantages and Disadvantages of Realistic Approach and Porous Approach for Closely Packed Pebbles in CFD Simulation," *Chemical Engineering Science*, **34** (2010)
2. J. GE, C. WANG, Y. XIAO, W. TIAN, S. QIU, et. al, "Thermal-hydraulic Analysis of a Fluoride-Salt-Cooled Pebble-Bed Reactor with CFD Methodology," *Progress in Nuclear Energy*, **91** (2016)
3. D. GASTON, C. PERMANN, J. PETERSON, A. SLAUGHTER, D. ANDRS et. al, "Physics-based Multiscale Coupling for Full Core Nuclear Reactor Simulation," *Annals of Nuclear Energy*, **84** (2015)
4. B. STOCKER and H. NIEBEN, "Data Sets of the SANA Experiment: 1994-1996," Forschungszentrum Julich Technical Report
5. E. ACHENBACH, "Heat and Flow Characteristics of Packed Beds," *Experimental Thermal and Fluid Sciences*, **10** (1995)

6. P. AVIGNI, "TRACE Loop Modeling of the Liquid Salt Test Loop", Oak Ridge National Laboratory Technical Report (2016)
7. D. VORTMEYER and J. SCHUSTER, "Evaluation of Steady Flow Profiles in Rectangular and Circular Packed Beds by a Variational Method," *Chemical Engineering Science*, **38** (1983)
8. E. YOU, F. CHEN, L. SHI, and Z. ZHANG, "An Improved Prediction Model for the Effective Thermal Conductivity of Compact Pebble Bed Reactors," *Nuclear Engineering and Design*, **323** (2017)
9. W. GRAY and K. O'NEILL, "On the General Equations for Flow in Porous Media and Their Reduction to Darcy's Law," *Water Resources Research*, **12** (1976)
10. A.J. NOVAK, L. ZOU, J.W. PETERSON, D. ANDRS, J. KELLY, R.N. SLAYBAUGH, R.C. MARTINEAU, and H.D. GOUGAR, "Pronghorn Theory Manual," Idaho National Laboratory Technical Report (2018)
11. C.G. DU TOIT, P.G. ROUSSEAU, G.P. GREYVENSTEIN, and W.A. LANDMAN, "A Systems CFD Model of a Packed Bed High Temperature Gas-Cooled Nuclear Reactor," *International Journal of Thermal Sciences*, **45** (2008)
12. D.A. KNOLL and D.E. KEYES, "Jacobian-free Newton-Krylov Methods: A Survery of Approaches and Applications," *Journal of Computational Physics*, **193** (2004)
13. Y. SAAD and M.H. SCHULTZ, "GMRES: A Generalized Minimum Residual Algorithm for Solving Nonsymmetric Linear Systems," *Journal of Scientific and Statistical Computing*, **7** (1986)
14. G.J. AUWERDA, Y. ZHENG, D. LATHOUWERS, and J.L. KLOOSTERMAN, "Effect of Non-Uniform Porosity Distribution on Thermal Hydraulics in a Pebble Bed Reactor," *Proceedings of NURETH-14* (2011)
15. H. HUAND and J. AYOUB, "Applicability of the Forchheimer Equation for Non-Darcy Flow in Porous Media," *Society of Petroleum Engineers* (2006)
16. R.M. FAND, B.Y.K. KIM, A.C.C. LAM, and R.T. PHAN, "Resistance to the Flow of Fluids Through Simple and Complex Porous Media Whose Matrices are Composed of Randomly Packed Spheres," *Transactions of the ASME*, **109** (1987)
17. KTA, "Reactor Core Design of High-Temperature Gas-Cooled Reactors Part 3: Loss of Pressure Through Friction in Pebble Bed Cores," 3102.3 (1981)
18. KTA, "Reactor Core Design of High-Temperature Gas-Cooled Reactors Part 2: Heat Transfer in Spherical Fuel Elements," 3102.2 (1981)
19. A. AMIRI and K. VAFAI, "Analysis of Dispersion Effects and Non-Thermal Equilibrium, Non-Darcian, Variable Porosity Incompressible Flow Through Porous Media," *International Journal of Heat and Mass Transfer*, **37** (1994)
20. E. TSOTSAS and H. MARTIN, "Thermal Conductivity of Packed Beds: A Review," *Chemical Engineering Processes*, **22** (1987)
21. G. BREITBACH and H. BARTHELS, "Radiant Heat Transfer in the HTR Core After Failure of the Afterheat Removal Systems," *Transactions of the American Nuclear Society*, **31** (1979)
22. "Heat Transport and Afterheat Removal for Gas Cooled Reactors Under Accident Conditions," IAEA-TECDOC-1163 (2000)
23. H. PETERSEN, "The Properties of Helium: Density, Specific Heats, Viscosity, and Thermal Conductivity at Pressures From 1 to 100 bar and From Room Temperature to About 1800 K," Danish Atomic Energy Commission (1970)
24. A.T.D. BUTLAND and R.J. MADDISON, "The Specific Heat of Graphite: An Evaluation of Measurements," *Journal of Nuclear Materials*, **49** (1973)
25. J. BAGGEMANN, D. SHI, S. KASSELMANN, S. KELM, H.J. ALLELEIN, and A. HURTADO, "Use of SANA Experimental Data for Validation and Verification of MGT-3D and a CFD Porous Media Model for VHTR Application," *Nuclear Engineering and Design*, **305** (2016)
26. A.E. SLAUGHTER, J.W. PETERSEN, D.R. GASTON, C.J. PERMANN, D. ANDRS, and J.M. MILLER, "Continuous Integration for Concurrent MOOSE Framework and Application Development on GitHub," *Journal of Open Research Software* (2015)
27. A. NOURI-BORUJERDI and S.I.T. GHOMSHEH, "An Improved Porous Media Approach to Thermal-Hydraulic Analysis of High-Temperature Gas-Cooled Reactors," *Annals of Nuclear Energy*, **76** (2015)
28. M. GIESE, K. ROTTSCHAFER, and D. VORTMEYER, "Measured and Modeled Superficial Flow Profiles in Packed Beds With Liquid Flow," *American Institute of Chemical Engineers Journal*, **44** (1998)
29. Y. FERNG and K. LIN, "Investigating Effects of BCC and FCC Arrangements on Flow and Heat Transfer Characteristics in Pebbles Through CFD Methodology," *Nuclear Engineering and Design*, **258** (2013)
30. H. PARK, D. A. KNOLL, D. R. GASTON, and R. C. MARTINEAU, "Tightly Coupled Multiphysics Algorithms for Pebble Bed Reactors," *Nuclear Science and Engineering*, **166** (2010)